A correlative study on the pore structure and water state of ancient decayed ivory from Sanxingdui site

Lang Jiang[1], Shilin Xiang[1], Yi Wang[1], Luman Jiang[2], Ning Wang[2], Leixu Tong[2], Lin Xiao[2], Qing Xiao[3], Fengjiao Wang[3], Lijuan Zhao[1]* and Jing Hong[1]*

[1]College of Chemistry and Materials Science, Sichuan Normal University, Chengdu, China, [2]Cultural Relics Conservation Center, Chengdu Institute of Cultural Relics and Archaeology, Chengdu, China, [3]Cultural Relics Conservation Center, Sichuan Province Institute of Cultural Relics and Archaeology, Chengdu, China

The discovery of a large number of ancient ivory and ivory artifacts in Sanxingdui site has elevated the importance of ancient ivory relics to the level of exploring the origins of Chinese civilization. To clarify the current preservation status of decayed ivory excavated from the Sanxingdui site, we have conducted an in-depth analysis of the structure-water state relationship of the ivory unearthed from the No. 4 sacrificial pit (K4) as an example. The research indicates that the ancient decayed ivory is composed of a mixed phase of hydroxyapatite [HA, $Ca_{10}(PO_4)_6(OH)_2$] and carbonated hydroxyapatite [CHA, $Ca_{10}(PO_4)_3(CO_3)_3(OH)_2$], which has a mixed structure of sheet-like and needle-like crystals. The organic fibrous protein within the ivory has basically disappeared, resulting in a porous structure with a porosity of approximately 39.2%. The pore size distribution is concentrated in the range of 2.5−100 nm, dominated by mesopores, with a handful of micropores. These pore structures are occupied by adsorbed water, free water and bound water, exhibiting a high water content (35%−40%). These water molecules play a filling and supporting role in the pore structure. During the dehydration and deterioration process of the ancient decayed ivory, the loss of water support results in internal stress within the microstructure of the ivory, leading to irreversible damage such as peeling, pulverization and cracking. The correlation study between the pore structure and water state of ancient decayed ivory provides clues for tracing the geological environment, sacrificial rituals, and ecological environments of ivories in ancient times, serving as a crucial window into Earth's history and biological evolution.

KEYWORDS

Sanxingdui site, no. 4 sacrificial pit, ancient decayed ivory, water state, pore structure

1 Introduction

The Sanxingdui Ruins (4.4–2.9 ka B.P.) is located on the south bank of the Yazi river, a tributary of the Tuojiang river in the northern Chengdu plain of China, which considered one of the significant archaeological discoveries of the 20th century

FIGURE 1
Distribution diagram of sacrifice pits at Sanxingdui site.

(Jingsong, 2005; Guo et al., 2023). A large quantity of cultural relics have been excavated since the excavation of Sanxingdui ruins, among which a relatively large number of ivory implements and entire ivory tusks have attracted worldwide attention (Chi, 2013; Yang and Xu, 2022). In particular, the ivory excavated from No. 4 sacrificial pit (K4) located in the central-northern part of the excavation area (Figure 1) exhibits significant traces of burning and severe mud degradation, resulting in poor preservation. Based on the radiocarbon dating of bamboo charcoal fragments from K4 (Bronk Ramsey, 2016; Reimer et al., 2020; Valášek et al., 2022), this pit belongs to the fifth phase of the Sanxingdui site, corresponding to the fourth phase of the Yin ruins culture, dating back approximately 3,000 years old (Zheng et al., 2013; Lai, 2015). The research on unique ivory excavated form K4 with serious argillation and burning marks is of crucial significance to unravel the origin of Yangtze River civilization and the code of ancient Shu's development.

It is well known that ivory is composed of pulp, pulp chamber, dentin (the main nucleus), cementum, and enamel. Ivory is a layered composite biomaterial of mineralized collagen fibers (MCF) consisting of hydroxyapatite (HA) and collagenous protein (Locke, 2008; Jantou-Morris et al., 2010). The specific arrangement of MCF is considered to be the reason for the optical and mechanical properties of ivory (Albéric et al., 2018). Since K4 belongs to the burning sacrificial pit, the organic components that play a bonding role in the ivory bones (mainly collagen and polysaccharides, accounting for about 30% of the total weight) have basically disappeared after high-temperature incineration and long-term burial, especially under the influence of adverse factors such as groundwater, soluble salts and microorganisms (Jackes et al., 2001; Figueiredo et al., 2010; Durga et al., 2022). With the degradation of organic collagen (Tranchant et al., 2023), the main inorganic residual body of the excavated ivory with severe mudding phenomena under the accumulation of backfill ash and the effect of exogenous remineralization (Godfrey et al., 2002; Lebon et al.,

2008; Figueiredo et al., 2010; Jantou-Morris et al., 2010; Virág, 2012), presenting a loose, porous, and fragile natura. It is universally acknowledged that the primary inorganic component of ivory is hydroxyapatite (HA), whose special stoichiometric composition is $Ca_5(PO_4)_{3-x}(CO_3)_x(F, Cl, OH)_y(CO_3)_{1-y}$ (Jantou-Morris et al., 2010; Virág, 2012; Durga et al., 2022). The ancient decayed ivory has undergone a complex transitions from burial to excavation to preservation, and the sudden change of preservation environment led to dehydration and brittle cracking of ivory. This indicates that the internal structure of the waterlogged cultural relics (including ancient decayed ivory) is closely related to water, and the change of internal structure directly affects the apparent properties of cultural relics.

Previously, relevant studies have more attention focused on the chemical composition and crystalline properties of ivory ontology (e.g., mammoth ivory and excavated ancient ivory) (Brody et al., 2001; Doménech-Carbó et al., 2016; Shen et al., 2021; Sun et al., 2022; Li et al., 2023). In addition, there have been numerous studies on the cultural value of ancient ivory, soil and microbial analysis, as well as reinforcement techniques (de Flamingh et al., 2020; Anczkiewicz et al., 2023; Lao et al., 2024), which provide valuable insights for the *in situ* protection of similar excavated artifacts. However, the interaction between the internal structure and water, as well as the effects on the structure and performance of the excavated waterlogged bone relics have not been studied.

Inspired by the research of the water existing states, water behavior, and structure within the porous waterlogged relics, including excavated waterlogged woods and soils (Hinshaw and Wohl, 2021; Guo et al., 2022; Li et al., 2022; Xu et al., 2022; Yan et al., 2022; Lu et al., 2023). This paper takes the core dentin of decayed ivory remnants excavated from Pit 4 of the Sanxingdui Ruins as the research object. The innovation establishes the correlation between pore structure and water state on the basis of the composition and crystal structure of the ancient decayed ivory. Through the detailed analysis of the

water content, water state and deterioration process caused by water continuously loss within the ancient decayed ivory, it providing a scientific basis for tracing the geological environment of ancient times, the culture of sacrificial burning, and the composition of ancient ivories' living environments. Simultaneously, it contributes a scientific archaeological research and utilization plan for ancient decayed bone and keratin artifacts.

2 Materials and methods

2.1 Samples

Carefully selected decayed ivory relics from the K4 area of the Sanxingdui Archaeological Site were sampled for research purposes. As illustrated in Figure 2, this figure not only depicts the temporary conservation environment of the ivory excavated from the Sanxingdui site (Figures 2A–C) but also showcases the actual photographs of selected K4 relic samples, with dentin as the primary focus of sampling (Figure 2D). The test samples are specifically labeled as K4YW-24, K4YW-28 and K4YW-35, along with K4YW-24-White and K4YW-24-Black, which are distinguished based on their marked differences in macroscopic morphology and coloration. Among them, K4YW-35 involves two parallel samples, labeled as K4YW-35-1 and K4YW-35-2. Specially, K4YW-24-White represents the inner layer of dentin exhibits no significant signs of burning or charring. K4YW-24-Black refers the outer layer of dentin displays prominent burning marks and appears charcoal-black in coloration.

2.2 Experimental methods

In dry-method testing, vacuum freeze-drying technology is adopted to conduct the corresponding pretreatment to preserve the original microscopic morphology of the samples as much as possible. In contrast, wet-method testing aims to maintain the original state of the samples (waterlogged ancient decayed ivory) for direct characterization and analytical research.

2.2.1 Chemical composition analysis

The chemical structure of freeze-dried ancient decayed ivory powder was tested using Fourier transform infrared spectroscopy (FTIR, VERTEX 70, Thermo Fisher Scientific Industrial Products Inc., United States) with a resolution of 4 cm^{-1} and a scanning range of 4,000-400 cm^{-1}. X-Ray photoelectron spectroscopy (XPS, ESCALAB Xi, Thermo Fisher Scientific, Al Kα radiation source, tube voltage of 40 kV, and tube current of 40 mA) was conducted to analyze the chemical valence states of the freeze-dried ancient decayed ivory powder. The distribution of chemical elements within the freeze-dried ancient decayed ivory was observed by energy dispersive X-ray spectroscopy (EDS, X-MAX^{N}50MM2, Carl Zeiss AG, operating voltage of 20 kV).

2.2.2 Crystal structure analysis

The crystal structure of the freeze-dried ancient decayed ivory powder was comprehensively characterized using X-ray powder diffraction (XRD, MiniFlex600 X, Rigaku Corporation, Japan, Cu Kα radiation, scanning speed of 10°/min, and scanning range of

2°-80°) and transmission electron microscope (TEM, HT7800, Hitachi, testing voltage of 120 kV).

2.2.3 Pore analysis

Dry porosity testing: The scanning electron microscope (SEM, Zeiss EV018, Carl Zeiss AG, operating voltage of 20 kV) was employed to initially analyze the pores of the freeze-dried ancient decayed ivory. The specific surface area (SSA) and pore size distribution of the freeze-dried ancient decayed ivory powder were measured using a fully automatic Brunauer-Emmett-Teller (BET) analyzer (ASAP2460, Micromeritics Instrument Corporation, United States) at a testing temperature of 77.3 K. The average pore diameter and porosity of the freeze-dried ancient decayed ivory were assessed using a high-performance automatic mercury intrusion porosimeter (MIP, Micromeritics Auto Pore IV 9,500, Micromeritics Instrument Corporation, United States).

Wet porosity testing: The MesoMR23-060H-I Low Field Nuclear Magnetic Resonance (LF-NMR) analyzer (Suzhou Niumai Analytical Instruments Co., Ltd.) was employed to investigate the waterlogged decayed ivory in its original state. The specific parameters were set to as a resonance frequency of 23 MHz, magnet strength of 0.5 T, coil diameter of 60 mm, and magnet temperature of 32°C.

2.2.4 Water content and moisture state analysis

Water content testing: The weight loss of ancient decayed ivory was measured by gravimetric method at different temperatures (25, 60 and 100°C). The water content of the samples was calculated according to Equation 1:

$$W_R = \frac{\Delta W}{W_0} \times 100\% \qquad (1)$$

Where $W_R = (W_0 - W_t)/W_0 = \Delta W/W_0$, with W_R representing the water content, W_0 representing the initial weight of the sample, W_t representing the constant weight of the sample after drying, and ΔW representing the weight reduction during drying. Each group of samples was tested in parallel three times.

Water state testing: The water content and moisture state of ancient decayed ivory was initially assessed using a thermal gravimetric analyzer (TGA, TGA Q500, TA Instruments, United States) under an N_2 atmosphere with a flow rate of 50 mL/min, and the temperature was raised from room temperature to 800°C at a heating rate of 10°C/min. The moisture status of the ancient decayed ivory was also evaluated by differential scanning calorimeter (DSC, PE8500, PerkinElmer Instruments, United States) with a heating rate of 2°C/min and a temperature range from 10°C to 100°C. To further analyze the moisture state of the ancient decayed ivory in depth, a detailed characterization was conducted by LF-NMR. Specific analysis parameters were set as follows: hard pulse 90°, pulse width (P1) 5.8 μs, hard pulse 180°, pulse width (P2) 10 μs, repetition sampling waiting time (TW) 5,500 ms, number of echoes (NECH) 18,000, number of repetitions (NS) 8, and receiver bandwidth (SW) 125 kHz. The obtained test data were then inverted 10,000 times, and plotted in the software to obtain the transverse relaxation time T_2 spectrum.

Water Loss and deterioration analysis: The water loss kinetics of the ancient decayed ivory was investigated using a fully automated dynamic vapor sorption (DVS) analyzer (Proumid SPSx, Proumid GmbH, Germany). The test was conducted at a constant temperature of 25°C, with a humidity range of 25%–95% RH and a humidity
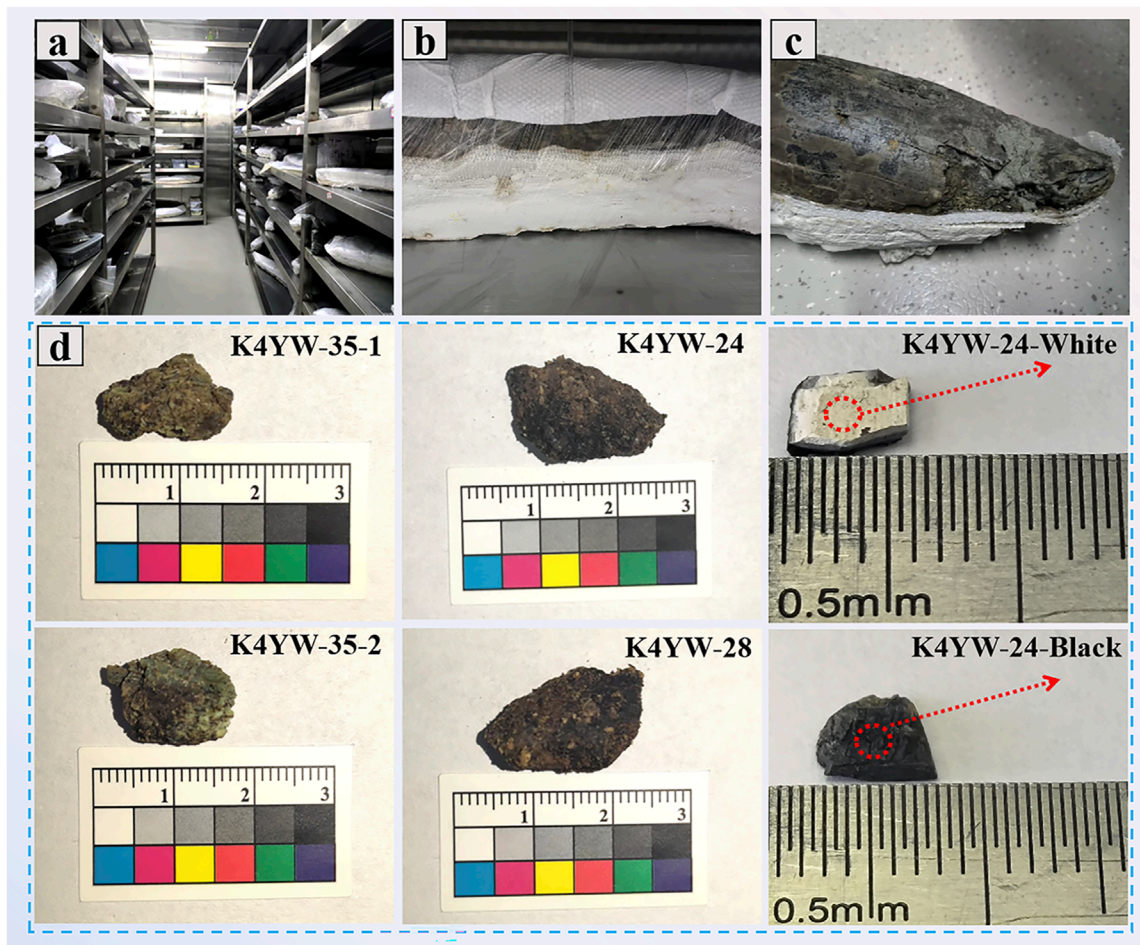
FIGURE 2
(A) The underground cold storage (4°C, 95% RH) of ivory excavated from the Sanxingdui. **(B)** Decayed ivory wrapped in polymer bandage and **(C)** partially exposed ivory. **(D)** Physical drawings of ivory fragments (K4YW-24, K4YW-28, K4YW-35-1, K4YW-35-2, K4YW-24-White and K4YW-24-Black) excavated from K4 at the Sanxingdui site.

gradient of 10% RH. In the testing process, the humidity was first decreased (from 95% to 25% RH) and then increased (from 25% to 95% RH). Combining the pore structure and moisture characteristics of the excavated ancient decayed ivory, the surface micromorphological evolution of the dentin for ivory during the water loss process was systematically observed and recorded at different time points under the experimental conditions of constant temperature of 25°C and relative humidity of 65% RH using a super depth-of-field three-dimensional microscope (VHX-2000C, Keyence, Japan) to verify the specific deterioration process of the ivory aggravated by the loss of water.

3 Results and discussion

3.1 Chemical composition and crystal structure analysis of ancient decayed ivory

Three parallel samples (K4-1, K4-2, K4-3) of ivory excavated from K4 was employed by FTIR, as shown in Figure 3A.

The characteristic peaks of the ivory excavated from K4 are basically consistent with those of HA (Piccini et al., 2021; Abdel-Maksoud et al., 2022; Li et al., 2023; Xu et al., 2024). In infrared spectroscopy, the characteristic peak at 962 cm^{-1} is attributed to the v_1 vibrational absorption peak of PO_4^{3-}; the absorption peak at 1,028 cm^{-1} corresponds to the v_3 vibrational absorption peak of phosphate ions; the infrared characteristic peak of 572 cm^{-1} is caused by the v_4 bending vibration of PO_4^{3-}, while the infrared characteristic peak at 471 cm^{-1} is the v_2 bending vibration peak of PO_4^{3-} (Liu et al., 2018; Li et al., 2023; Scaggion et al., 2024). The peak at 1,647 cm^{-1} indicates the bending vibration of organic -OH or N-H groups. Lastly, the absorption peak at 3,627 cm^{-1} is attributed to the stretching vibration of O-H bonds (Islam et al., 2011; Marcomini et al., 2016). It is noteworthy that the absorption peak at 1,434 cm^{-1} unequivocally indicates the v_3 vibrational absorption characteristic of CO_3^{2-}, despite its relatively weak intensity. Considering the complexity of the burial and excavation environments that the excavated ancient ivory has endured, coupled with the potential for prior burning treatment (Vargas-Becerril et al., 2018). It is reasonable to deduce that the ivory

samples retrieved from the K4 site may contain minor amounts of mixed substitution type for carbonated hydroxyapatite with varying degrees of carbonate substitution (Elliott, 1969; Pebriani and Sari, 2019). The chemical valence state and content of K4YW-24 was further employed by XPS (Figures 3B, C). The signals of C, N, O, P, Ca, and Cu can be detected from the XPS survey spectrum of K4YW-24, of which O content exhibits the highest (~65 at%). Both the contents of N and Cu elements are less than 1 at%. The XPS spectra analysis of the C, O and P elements in the K4YW-24 sample revealed that, in addition to the standard C-C bond peak at 284.8 eV (Bandara et al., 2020), a prominent peak is observed at 288.2 eV in the C element spectrum (Xia et al., 2019), indicating the presence of CO_3^{2-} (Supplementary Figure S1). Furthermore, the characteristic peak at 530.7 eV in the O element spectrum is attributed to the combined contribution of CO_3^{2-} and inorganic salts such as phosphates (Yu et al., 2023), which provides further confirmation of the presence of CO_3^{2-} and PO_4^{3-} in the excavated ancient ivory. After undergoing sacrificial burning and thousands of years of burial evolution, the structure of the decayed ivory excavated from K4 is loose, and the preserved components are primarily inorganic component. This is also one of the reasons why the ancient decayed ivory is prone to cracking and pulverization after dehydration.

Due to the unique burial environment, the element distribution of the decayed ivory excavated from K4 exhibits variations. As shown in Figures 3D, E, the optical images of K4YW-24 reveal significant differences in burning traces. EDS results indicate that ivory contains a certain amount of C, N, O, P, and Ca elements whether or not it is incinerated, but their special elemental distribution and content differ (Supplementary Figure S2). The uneven distribution of C elements in the ivory excavated from K4, with the presence of residual carbon agglomeration, which may be attributed to the uneven carbonization of the ivory exterior after burning, resulting in excessively high elemental content in localized areas.

The XRD spectrum of decayed ivory excavated from different K4 is shown in Figures 4A, B. The diffraction peak positions of three parallel samples of K4YW-24 (K4YW-24-1, K4YW-24-2, and K4YW-24-3) and K4YW-28 (K4YW-28-1, K4YW-28-2, and K4YW-28-3) are roughly the same. The main diffraction peaks of K4YW-24 and K4YW-28 are basically consistent with the carbonated hydroxyapatite standard (JCDPS: PDF# 19-0272) (Pebriani and Sari, 2019), which also verifies that the decayed ivory unearthed from K4 contains carbonated hydroxyapatite. Notably, there are some differences in the additional diffraction peaks of K4YW-24 at 20.9°, 26.7°, 42.5°, 60.2° and 63.8° compared to those of K4YW-28 at 19.78°, 61.9° and 64.1°. These variations may be attributed to impurities generated after the burning of the decayed ivory excavated from K4, or they could stem from individual differences among ivory specimens. Existing studies have shown that the crystallinity of carbonated hydroxyapatite can be reflected by the full width at half maximum (FWHM) of the ~26.0° (002) diffraction peak, which means that the smaller the FWHM value of ~26.0° (002), the higher the crystallinity is (Zheng et al., 2017; Montoya-Escobar et al., 2022). The average FWHM values of the ~26.0° (002) diffraction peak for three parallel samples of K4YW-24 and K4YW-28 are 0.259 ± 0.015 and 0.231 ± 0.040, respectively (Supplementary Table S1; Figure 4C), indicating that the crystallinity of K4YW-28 ivory is slightly higher. The Scherrer

equation can be used to calculate the crystallite size of samples (Kostov-Kytin et al., 2018; Rabiei et al., 2020; Jaswal et al., 2023). The effective average crystallite size (D) of the excavated decayed ivory is evaluated by Equation 2:

$$D = \frac{K\lambda}{\beta \cos \theta} \qquad (2)$$

Where D represents the crystal size in nanometers, β is the FWHM in radians, θ is the Bragg diffraction angle, λ is the wavelength of the X-ray, and K is a constant (usually 0.89). The average crystallite sizes of K4YW-24 and K4YW-28 at (002) crystal plane are 32.365 ± 0.179 and 34.208 ± 0.299 nm, respectively (Supplementary Table S2; Figure 4C). The effective average crystallite size of K4YW-28 is larger than that of K4YW-24. This observation corroborates the previous finding that the higher crystallinity of K4YW-28 leads to a corresponding increase in crystallite size.

To further investigate the crystal structure of the K4 ancient decayed ivory, the K4YW-24 sample was characterized by TEM (Figures 4D–I). The mixed morphology of two crystals stacked together, within K4YW-24 contains primarily of a lamellar structure, secondarily with a needle-like structure (Figures 4D–F). The HRTEM image of K4YW-24 reveals interplanar spacings of 0.240, 0.263, 0.268 and 0.320 nm (Figure 4H), respectively, corresponding to the crystal planes (301), (202), (300) and (102) of carbonated hydroxyapatite (van Rijt et al., 2021). Additionally, the selected area electron diffraction (SAED) pattern of K4YW-24 is depicted in Figure 4G. The diffraction rings in the pattern correspond to the crystal planes (002) and (202) of carbonated hydroxyapatite. Meanwhile, the crystal planes (101), (110) and (104) are consistent with the standard crystal planes of hydroxyapatite (Zheng et al., 2017). These results indicate that the decayed ivory excavated from K4 contains carbonated hydroxyapatite crystals. After burning sacrifices and long-term high-humidity burial environment, the ivory crystals aggregate under the exogenous remineralization (Godfrey et al., 2002; Lebon et al., 2008; Figueiredo et al., 2010; Jantou-Morris et al., 2010; Virág, 2012; Doménech-Carbó et al., 2016), primarily manifesting in a lamellar stacked morphology.

3.2 Pore structure analysis of ancient decayed ivory

The decayed ivory excavated from K4 belongs to a class of porous materials. The environmental temperature and humidity change during the excavation and preservation of ancient decayed ivory, the free water stored in its pores may undergo phase transition, volatilizing and migrating in the form of water vapor. In addition to the decomposition of organic collagen during the burial process (López-Costas et al., 2016; Tranchant et al., 2023) and the exogenous promotion of remineralization (Godfrey et al., 2002; Lebon et al., 2008; Figueiredo et al., 2010; Jantou-Morris et al., 2010; Virág, 2012; Doménech-Carbó et al., 2016), these factors also contribute to the unique multi-level structure of the ancient decayed ivory. Water evaporation or dehydration of the ancient decayed ivory can exacerbate the occurrence of cracks and even pulverization damage. Microscopic pore structure analysis of ancient decayed ivory excavated from K4 was conducted by both dry methods
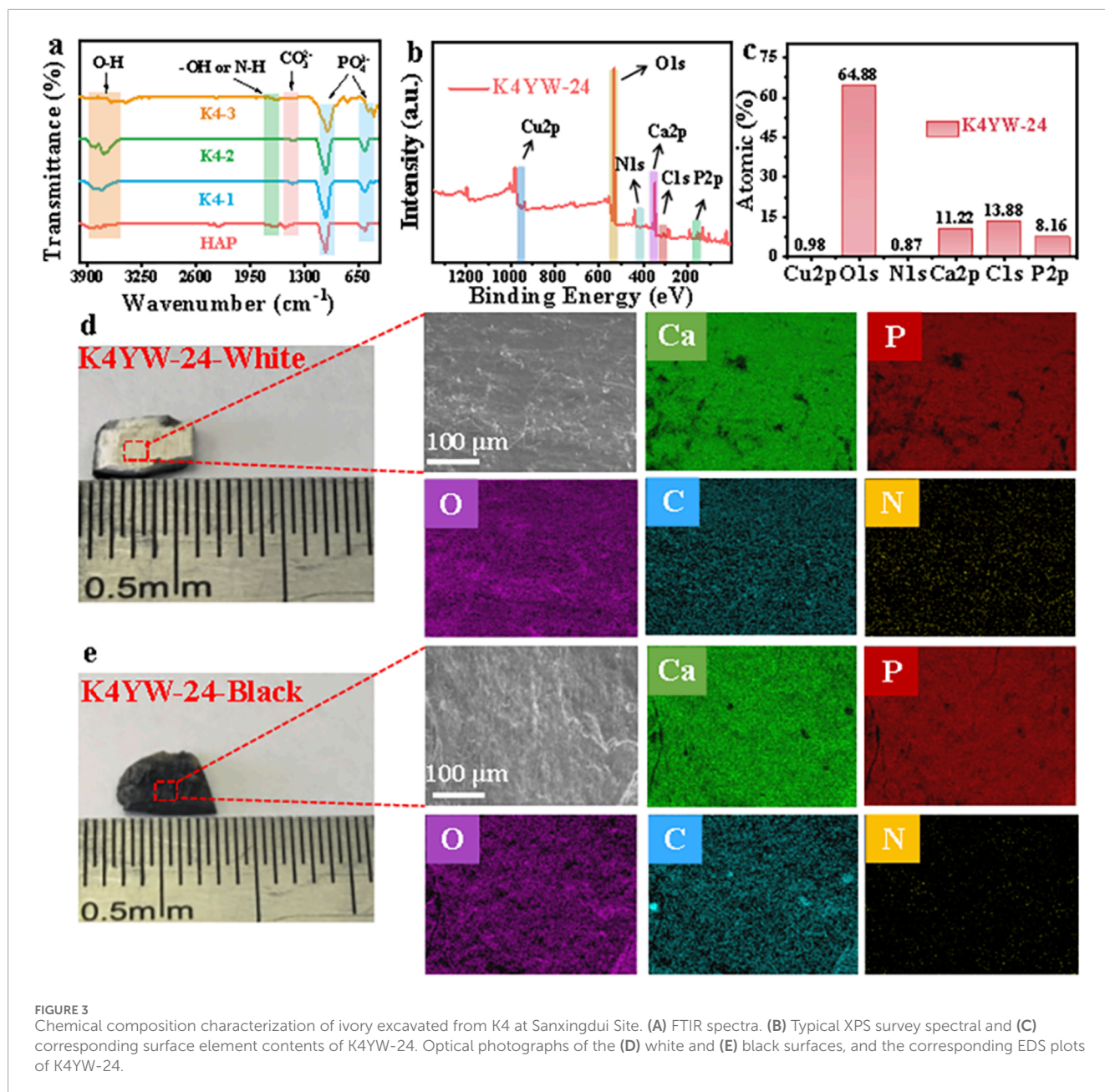
FIGURE 3
Chemical composition characterization of ivory excavated from K4 at Sanxingdui Site. **(A)** FTIR spectra. **(B)** Typical XPS survey spectral and **(C)** corresponding surface element contents of K4YW-24. Optical photographs of the **(D)** white and **(E)** black surfaces, and the corresponding EDS plots of K4YW-24.

(e.g., SEM, BET and MIP) and wet methods (e.g., LF-NMR). The micro-morphology of K4YW-24 exhibits prominent cracks and pores (Figures 5A, D). The pore size distribution of K4YW-24 varies regionally and widely, ranging from a few hundred nanometers (0.643 ± 0.166 μm, Figure 5B) to several micrometers (4.878 ± 2.054 μm, Figure 5E). Based on the cylindrical model, MIP exhibits significant errors in testing micropores and small pores, while demonstrating high accuracy in analyzing macropore pore sizes (Papynov et al., 2018). Therefore, the pore size distribution, average pore size and porosity of K4YW-24 were measured by MIP, as depicted in Figures 5C, F. The pore sizes of K4YW-24 can be classified into macropores and mesopores, with the overall pore size mainly distributed between 5 and 100 nm. The distribution rang of macropore structures is wide, with a relatively

low porosity (~39.2%), which may be attributed to the impurities filling the internal pores or structural collapse occurring during the incineration process of the excavated decayed ivory from K4.

Currently, nitrogen physical adsorption method can effectively characterize the pore size distribution of micropores or mesopores of materials (Kuila and Prasad, 2013). As shown in Figure 5G, the adsorption-desorption curves of K4YW-24 and K4YW-28 belongs to typical type IV isothermal adsorption-desorption curves. The pore size distribution of K4YW-24 and K4YW-28 is primarily concentrated within the mesopore range (2–50 nm, Figure 5H). However, both samples also contain a small amount of macropores with pore sizes between 50 and 100 nm, as well as a certain quantity of micropores (<2 nm). The specific surface areas of K4YW-24 and K4YW-28 are 135.8 and 87.11 m^2/g, respectively, with an average
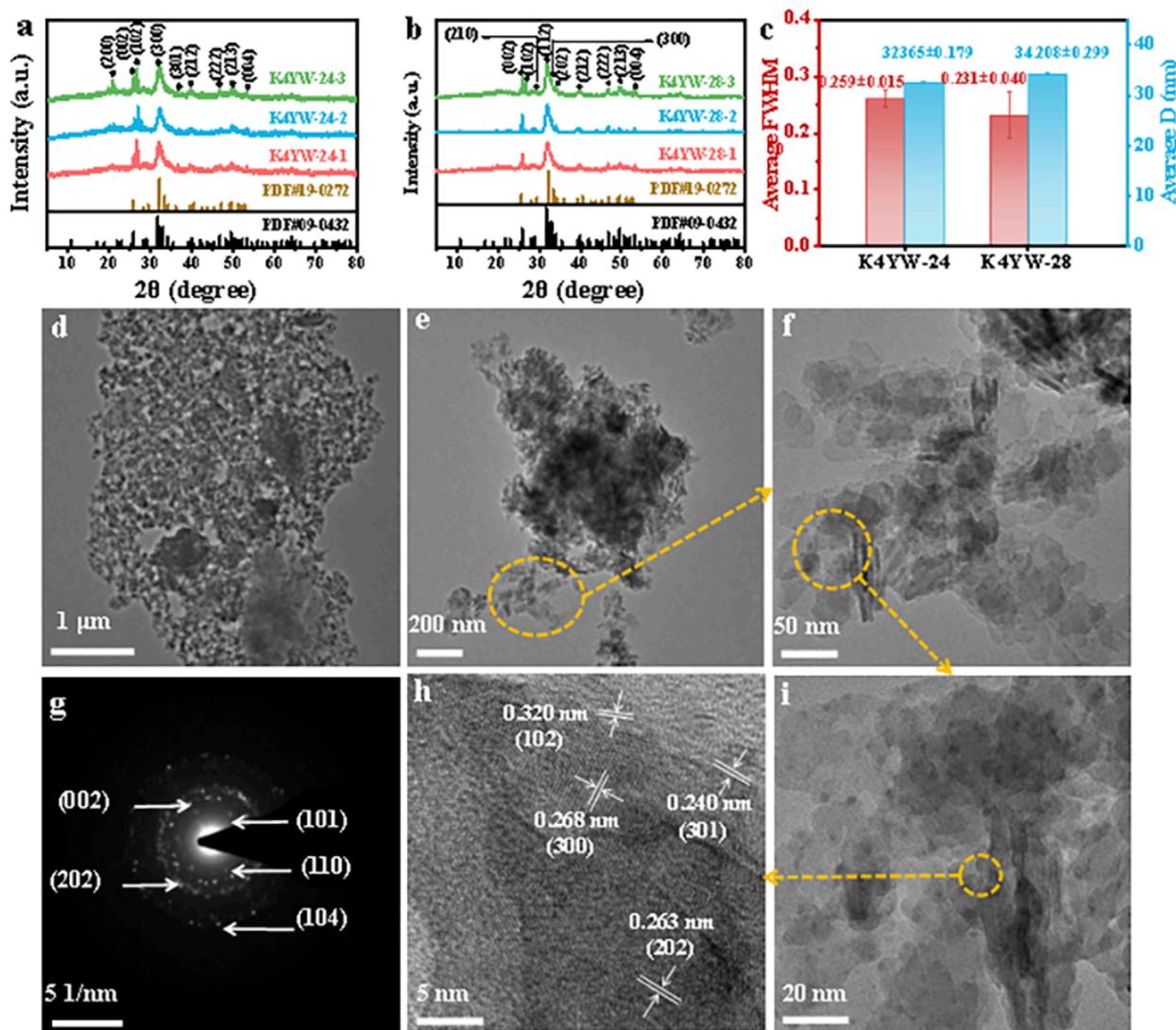
FIGURE 4
XRD patterns of **(A)** K4YW-24 and **(B)** K4YW-28. **(C)** The average FWHM and crystallite size corresponding to K4YW24 and K4YW-28 at (002) crystal plane. TEM at **(D–F, I, H)** different magnification. **(G)** SAED image and **(H)** HRTEM image of K4YW-24.

pore size of 16.68 and 11.89 nm (Figure 5I). This indicates that the specific surface areas and average pore diameters of ancient decayed ivory from different excavation sites in K4 are vary different, and the pore diameters of ancient decayed ivory exhibit irregular phenomena due to these factors such as specific burial environment, the age of the ivory, and the sampling position. The results of dry tests can provide a certain basis for the selection of dehydration and reinforcement materials for the ancient decayed ivory. However, dry pore testing has some limitations, such as irreversible damage to wet cultural relics during the drying process and the collapse of some small pores. To further reveal the true internal pore structure of water-containing ancient decayed ivory, LF-NMR testing can be employed to analyze the pore structure of ivory while adhering to the "minimum intervention principle" of cultural relic protection.

LF-NMR technology has been flourishing in recent years in the fields of polymer materials and life sciences due to its non-destructive, non-invasive, accurate and rapid analytical advantages (Volkov et al., 2018; Zhang et al., 2022). The ivory excavated from the Sanxingdui Ruins is in a "water-saturated" state, which is prone to dehydrate, crack and pulverize after excavation. In order to more accurately reflect the internal pore structure of the ancient decayed ivory itself, the pores was characterized by LF-NMR. The porosity of K4YW-35 is relatively high, about 79%, with a lower solid density (Figure 6A). K4YW-35's pore radius is mainly concentrated between 2.5–100 nm (~83.44%), primarily consisting of macropores (>50 nm) and mesopores (2.5–25 nm, ~65.02%), with a small amount of micropores (<2 nm, ~3.21%). This indicates that the pore size distribution trends of the ancient decayed ivory from K4 are roughly consistent under wet and dry porosity tests, but there are certain differences in the pores. This is due to the fact that K4 belongs to a sacrificial pit involving incineration rituals, wherein the burial environment is loose and muddy. Consequently,
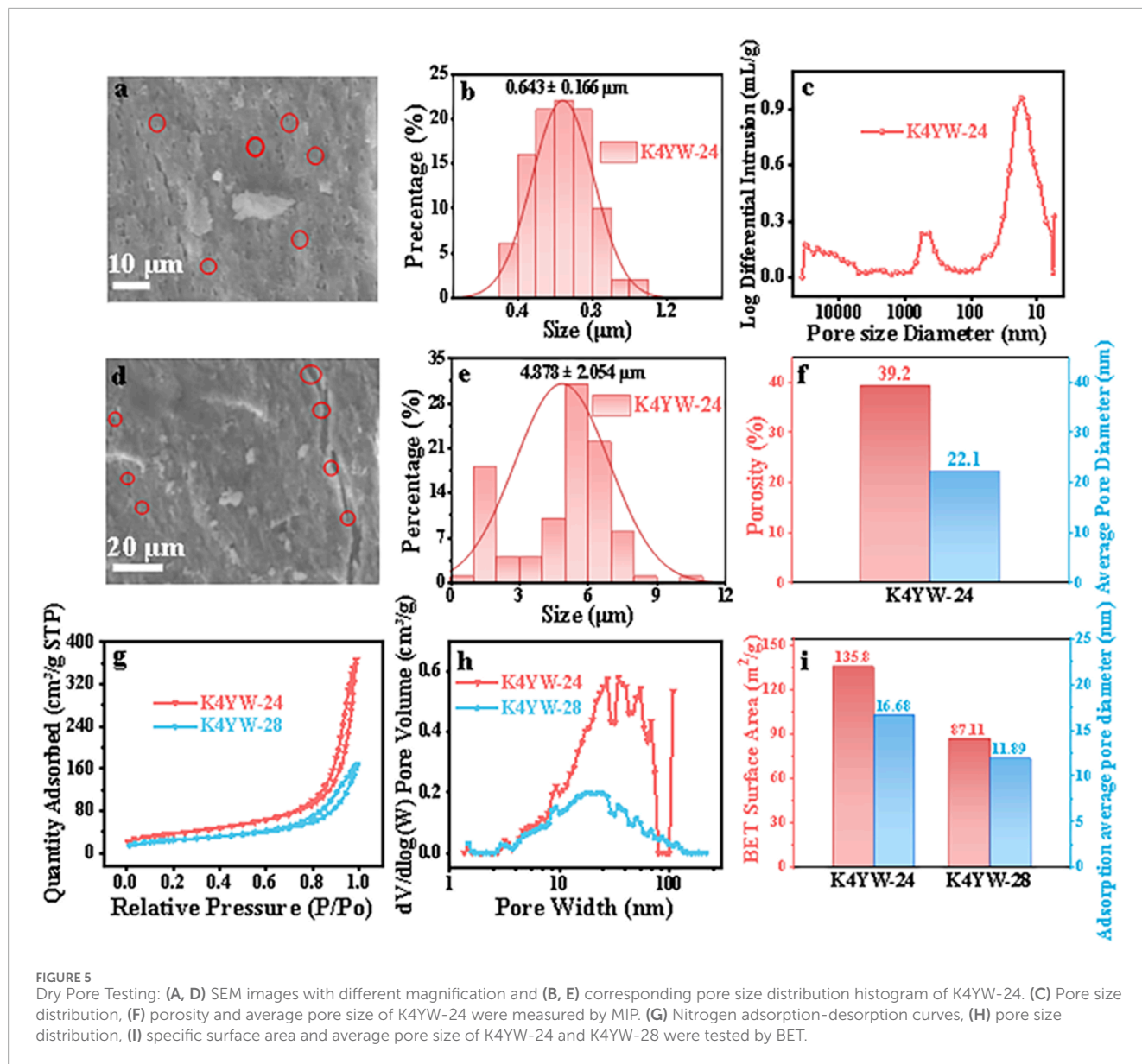
FIGURE 5
Dry Pore Testing: **(A, D)** SEM images with different magnification and **(B, E)** corresponding pore size distribution histogram of K4YW-24. **(C)** Pore size distribution, **(F)** porosity and average pore size of K4YW-24 were measured by MIP. **(G)** Nitrogen adsorption-desorption curves, **(H)** pore size distribution, **(I)** specific surface area and average pore size of K4YW-24 and K4YW-28 were tested by BET.

the diverse pore structures of the ivory itself are further accentuated by the burial conditions, failing to exhibit a certain regularity.

3.3 Water content and moisture status of K4 ancient decayed ivory

The organic matter of the ivory gradually decomposed in the long-term damp burial environment at the Sanxingdui Ruins, leaving internal cavities or microporous structures saturated with water. These structures exhibit a high water content, and water can replace the organic matter to balance the structure of the ivory. After the excavation, the ivory was found to quickly crack upon exposure to air. The original cracks gradually widen, undergo layering, cracking, peeling, weathering from the surface to the interior, and finally completely pulverize. Therefore, water loss is one of the key factors that affect the deterioration and evolution of

ancient decayed ivory. The dynamic water loss curves of K4YW-28 at 25, 60 and 100°C were monitored by gravimetric method to find out the water loss rate and water content (Figures 7A, B). Due to the loose structure of excavated ancient decayed ivory, the higher the heating temperature, the faster the water loss rate of K4YW-28 occurs. Specifically, for K4YW-28, achieving a constant weight through water loss requires 2, 4.5, and 24 h respectively at 100, 60, and 25°C (Figure 7A). Additionally, the moisture content of K4YW-28 exhibits a certain degree of variation (ranging from 35%-40%) under different temperature conditions (Figure 7B), which is likely attributed to the varying specific forms or states of water loss occurring under these distinct temperature states.

The water content of ancient decayed ivory was characterized using TG and DSC (Figures 7C, D). The TG curve of K4YW-35 exhibits a prominent and rapid decomposition phase (−43.55%) from room temperature to 126°C (Figure 7C), corresponding to the loss of free and adsorbed water. However, it is worth noting

FIGURE 6
Wet Pore Testing: **(A)** Porosity distribution map, **(B)** pore radius distribution curve and **(C)** pore radius distribution histogram of K4YW-35.

FIGURE 7
(A) Water loss curves and **(B)** corresponding water content of K4YW-28 at 25, 60, and 100°C. **(C)** TG-DTG curves, **(D)** DSC curves, **(E)** LF-NMR T2 relaxation spectroscopy, and **(F)** different moisture states content of K4YW-35.
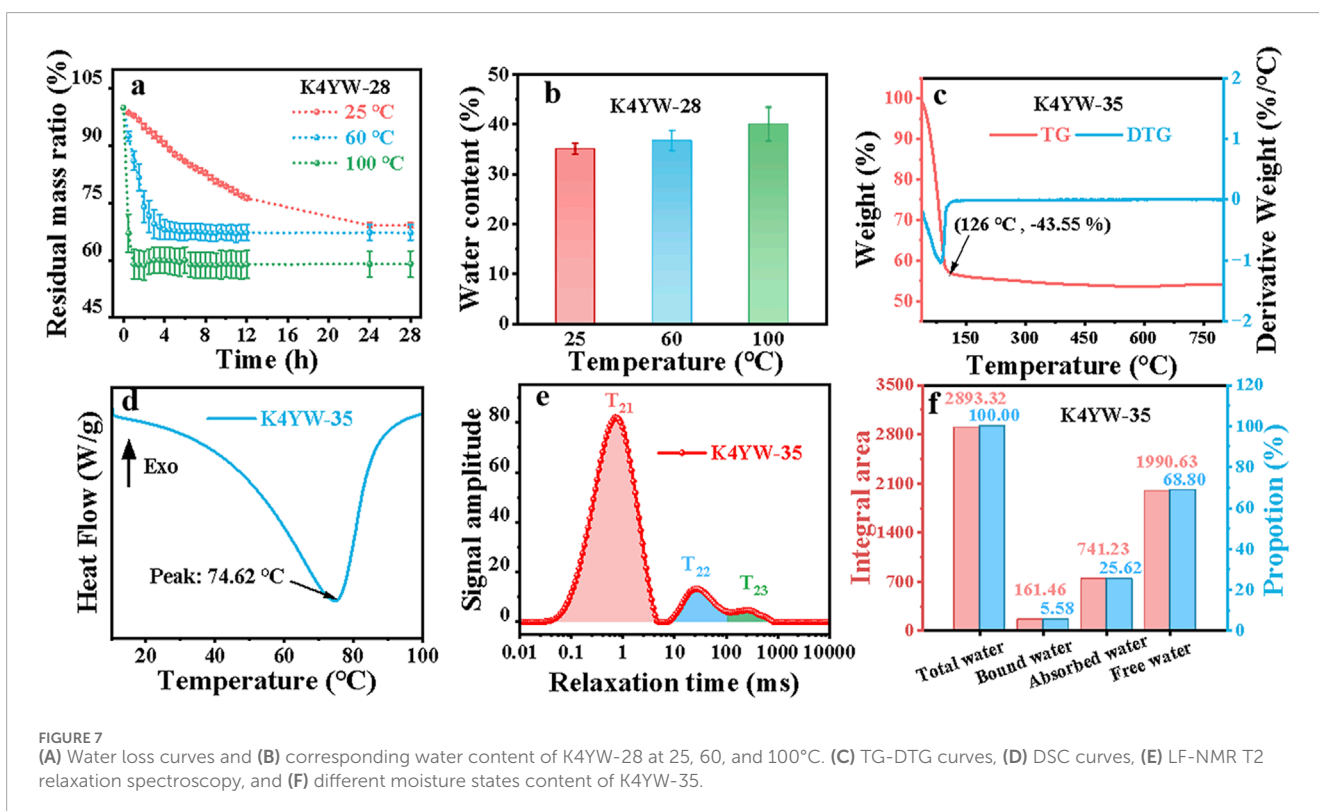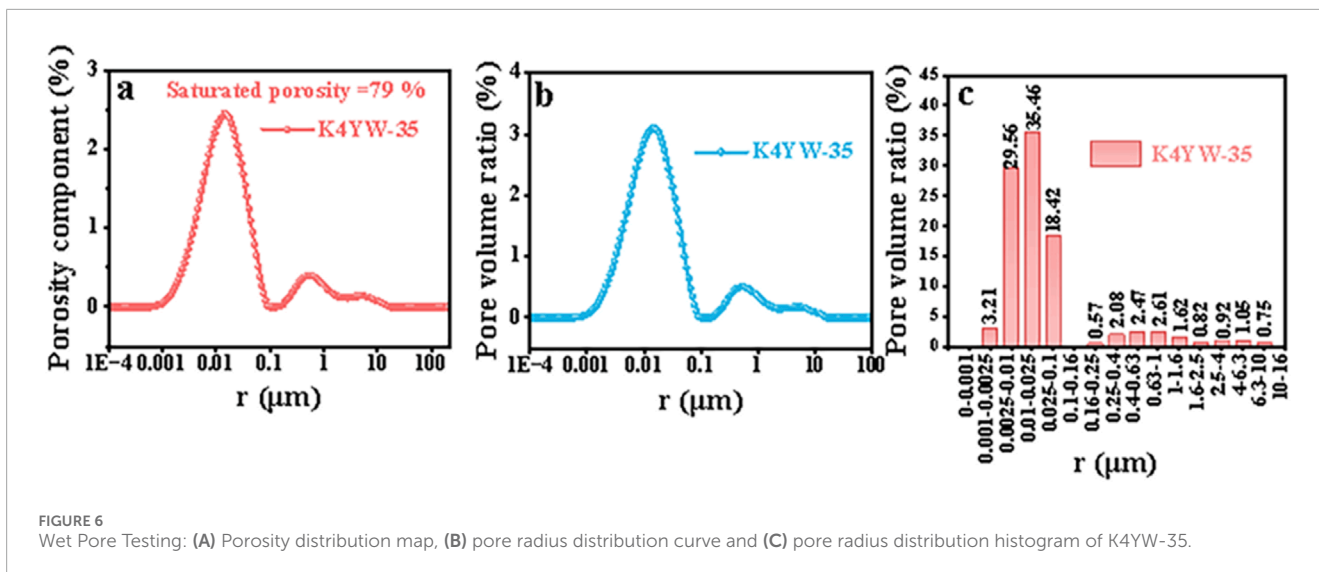
that due to the differences in the blocks of excavated ancient ivory, its water content will present a range value. The DSC curve displays a single endothermic peak at 74.62°C (Figure 7D), which is typically associated with the evaporation of free and adsorbed water (Yan et al., 2018).

There have been research reports on the utilization of nuclear magnetic resonance (NMR) technology to investigate the water state, water migration, and pore structure of porous materials, including waterlogged wooden relics (Penvern et al., 2020; Zhu et al., 2021). However, the water properties of waterlogged ancient decayed

ivory have not yet been unexplored. The water characteristics within waterlogged ancient decayed ivory can be rapidly and non-destructively investigated using LF-NMR by adopting ^{1}H protons in water as probes. The spin-spin relaxation time is also known as transverse relaxation time, denoted as T_2. The higher the T_2 value, the greater the proton's freedom, the stronger the water molecule mobility, and the easier it is expelled. The lower the T_2 value, the smaller the proton's freedom, the tighter the binding between water and substances, the poorer the water molecule mobility, and the more difficult it is to be expelled (Lv et al., 2018).
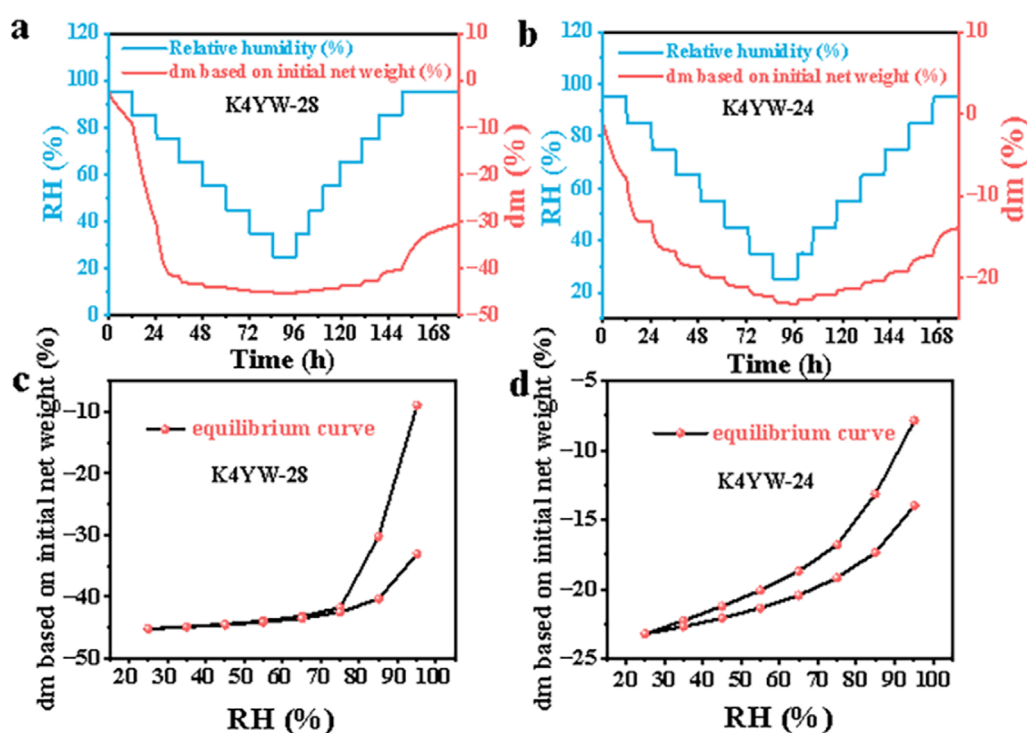
FIGURE 8
(A, B) Dynamic Moisture Adsorption curves and (C, D) corresponding weight curves of K4YW-28 and K4YW-24.

The signal amplitude in the T_2 spectrum reflects the peak area, which in turn reflects the water content. In the T_2 spectrum of K4YW-35, three distinct relaxation peaks represent different states of water: T_{21} (0.1–10 ms) corresponds to bound water, which is tightly bound to HA minerals, exhibiting poor mobility; T_{22} (10-100 ms) represents adsorbed water, displaying moderate mobility; whereas T_{23} (>100 ms) signifies free water, predominantly found in internal cavities, large cracks and dentin tubule macropores, characterized by high mobility, making it susceptible to external environmental factors and readily available for microbial utilization. It can be found that K4YW-35 has the highest content of free water (~68.80%) and the lowest content of bound water (~5.58%) (Figures 7E, F) (Guan et al., 2023; Zhu et al., 2023). This result indicates that most of the pore structure of the ancient decayed ivory are occupied by free water and adsorbed water. The small amount of bound water also indirectly verified the uniqueness of the burial environment (incineration ritual) of the ancient decayed ivory from K4. After incineration and long-term burial damp environment, the decomposition of organic collagenous protein components and the exogenous remineralization process may resulted in the generation of a small amount of bound water in ancient decayed ivory.

3.4 Water loss and deterioration of ancient decayed ivory

Since the excavation, the waterlogged ivory buried at Sanxingdui site has been faced with the irreversible deterioration damage due to lose water. The water loss kinetics of K4YW-28 and K4YW-24 under

a gradient humidity range of 95% to 25% RH at 25°C were measured by DVS analyzer. As illustrated in Figures 8A–D, during the overall humidity reduction, the weight of ancient decayed ivory continues to decline even during the platform stability period. After the stage of increasing environmental humidity, the ancient decayed ivory has a certain amount of water absorption and weight gain. Even when the humidity reaches 95% RH, it continues to slowly and slightly increase weight. Compared with the initial ancient decayed ivory, the weight of the ancient decayed ivory after DVS test decreased significantly. In particular, the weights of K4YW-28 and K4YW-24 are reduced by approximately 30.7% and 13.9%, respectively. This indicates that the dynamic process of dehumidification and humidification in ancient decayed ivory cannot be restored to its initial state. During the process of humidity reduction, the loss of internal water within the ancient decayed ivory can led to partial collapse of its internal structure and irreversible damage.

Due to the small depth of field and the imperceptible boundary between clear and blurred areas in microscopes, it becomes challenging to accurately measure the height of an object that exceeds the depth of field range (Sun et al., 2023). To address this issue, super-depth-of-field microscope was used to observe the dehydration process of the ancient decayed ivory fragments at 25°C and 65% RH. The surface changes of the same area in ancient decayed ivory after 0, 2, 5 and 24 h were observed using ×200 magnification super-depth imaging to explore the degree of dehydration deterioration. As shown in Figure 9, with the increase in water loss time, the surface of the K4YW-28 became progressively drier, exhibiting partial pulverization, shedding, and deepening of the original cracks. This may be related to the unique

FIGURE 9
Ultra-depth-of-field microscope images of three parallel samples of K4YW-28 (K4YW-28-1, K4YW-28-2 and K4YW-28-3) for different periods of continuous water loss at 25°C and 65% RH.
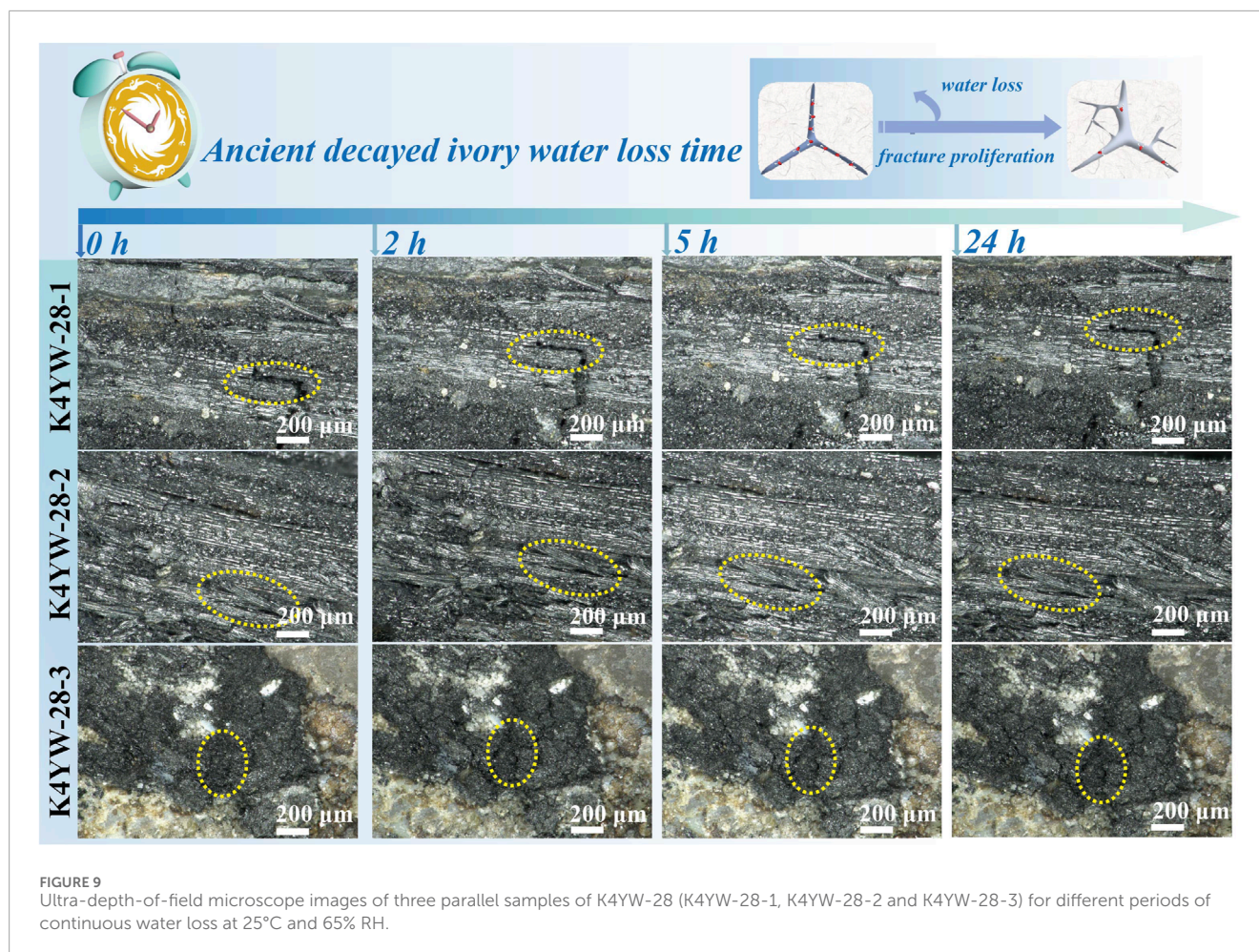
burial environment and special structure of the ancient decayed ivory. After incineration and burial, K4YW-28 exhibits a looser structure, resulting in a faster water loss rate and a greater degree of deterioration at room temperature. According to the T_2 spectra of K4YW-28 at 0 and 24 h water loss (25°C, 65% RH), respectively (Supplementary Figure S3), it is evident that after 24 h of supporting water loss, the residual water within the ivory primarily exists in the form of bound water, accompanied by a significant decrease in porosity (from 44.83% to 28.32%) (Supplementary Figure S3c). This observation directly supports the hypothesis that water loss leads to alterations in the hierarchical structure of ivory, adjustments in pore distribution, and ultimately macroscopic deterioration.

3.5 A correlation study on pore structure and moisture status of ancient decayed ivory

The K4 at the Sanxingdui Ruins is a sacrificial artifact burial pit formed based on a sudden event. A large number of water-filled pore structures and irregular cracks within ancient decayed ivory during the low-temperature and high humidity burial process of over 3,000 years, which is cased by the decomposition of organic collagen

fibers (Beasley et al., 2014; Tranchant et al., 2023) and the external promotion of remineralization (Godfrey et al., 2002; Lebon et al., 2008; Figueiredo et al., 2010; Jantou-Morris et al., 2010; Virág, 2012; Doménech-Carbó et al., 2016) have been formed. The correlation between the internal pore structure and moisture status of ancient decayed ivory is shown in Figure 10. The internal cavities, large cracks and large pore structures of ancient decayed ivory are mainly contain free water with good fluidity, which can be utilized by microorganisms. The pore structure of general size in ancient decayed ivory is mainly contains adsorbed water with moderate fluidity, which can be adsorbed on the surface of the material. Water molecules that are tightly bound to inorganic minerals through hydrogen bonds are also called bound water and have poor fluidity. It is suggested that the bound water may exist in the micro-nano pores and capillaries, or between mineral particles of ancient decayed ivory. The high water content of ancient decayed ivory can replace organic matter and play a role in structural balance. Ancient decayed ivory exposed to air will crack quickly on its surface and the original cracks will gradually widen due to moisture loss. Layering, cracking, peeling, and weathering occur from the surface to the interior of the ancient decayed ivory, ultimately leading to complete pulverization. Hence, the water migration results in severe deterioration of the structure and properties of ancient decayed ivory. The water migration is closely related to the internal pore structure and the corresponding moisture state contained in the ancient decayed ivory.
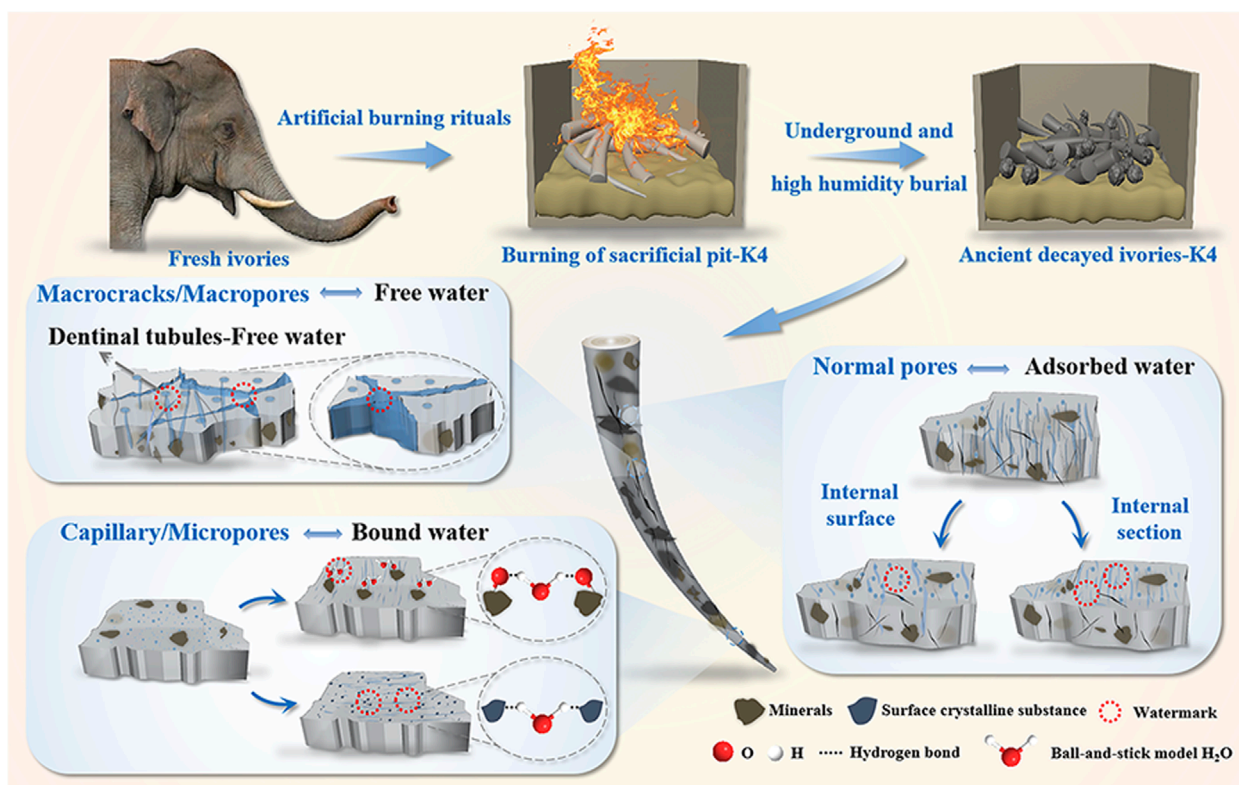
FIGURE 10
Schematic representation of the pore structure and moisture state relationships of decayed ivory excavated from K4.

4 Conclusion

After sacrificial burning and long-term underground burial, the ancient decayed ivory from K4 suffers from various degrees of water saturation, decay, incompleteness, fracture, discoloration, surface pulverization and peeling, as well as lamellar exfoliation, resulting in low strength and poor preservation conditions. Based on the correlation study between pore structure and moisture state of ancient decayed ivory, it is shown that the ancient decayed ivory is composed of a mixed phase of HA and CHA, which has a mixed structure of sheet-like and needle-like crystals. The organic protein components within the MCF layered structure of ancient decayed ivory have been largely degraded, forming a pore structure with a porosity of approximately 39.2%. The pore size distribution of ancient decayed ivory is concentrated in 2.5–100 nm (~83.44%), mainly mesoporous (2.5–25 nm, ~65.02%), and there are a small number of micropores (<2 nm, ~3.21%). These macropore and mesoporous are occupied by a large amount of free water (~68.80%) and adsorbed water (~25.62%), resulting in a high water content (35%–40%). In addition, there is a small amount of bound water (~5.58%) that tightly binds with inorganic minerals through hydrogen bonds. These occupying water play a filling and supporting role in the stable structure of the ancient decayed ivory. During the dehydration and deterioration process of ancient decayed ivory, the loss of water support leads to the generation of internal stress in its microstructure, eventually resulting in cracking, deformation, shedding, and pulverization. This ultimately causes irreversible damage to the structure and performance of the ancient decayed ivory. Research on the correlation between pore structure and water state of the ancient decayed ivory provides clues for tracing the geological environment, sacrificial rituals, and ecological environments of ivories in ancient times, serving as a crucial window into Earth's history and biological evolution. Additionally, it offers new insights for archaeological research of fragile bone and keratin artifacts excavated from archaeological sites .

Data availability statement

The original contributions presented in the study are included in the article/Supplementary Material, further inquiries can be directed to the corresponding authors.

Author contributions

LaJ: Conceptualization, Data curation, Formal Analysis, Investigation, Software, Visualization, Writing–original draft. SX: Formal Analysis, Writing–original draft. YW: Supervision, Writing–review and editing. LuJ: Formal Analysis, Investigation, Writing–review and editing. NW: Conceptualization, Writing–review and editing. LT: Conceptualization, Investigation, Writing–review and editing. LX: Conceptualization, Supervision, Writing–review and editing. QX: Conceptualization, Supervision, Writing–review and editing. FW: Conceptualization, Supervision,

Writing–review and editing. LZ: Conceptualization, Funding acquisition, Resources, Supervision, Writing–review and editing. JH: Conceptualization, Formal Analysis, Methodology, Resources, Supervision, Writing–review and editing.

Conflict of interest

The authors declare that the research was conducted in the absence of any commercial or financial relationships that could be construed as a potential conflict of interest.

Publisher's note

All claims expressed in this article are solely those of the authors and do not necessarily represent those of their affiliated organizations, or those of the publisher, the editors and the reviewers. Any product that may be evaluated in this article, or claim that may be made by its manufacturer, is not guaranteed or endorsed by the publisher.

Supplementary material

The Supplementary Material for this article can be found online at: https://www.frontiersin.org/articles/10.3389/feart.2024.1489898/full#supplementary-material

References

Abdel-Maksoud, G., Sobh, R. A., and Tarek, A. (2022). Evaluation of MMI/acrylate nanocomposite with hydroxyapatite as a novel paste for gap filling of archaeological bones. *J. Cult. Herit.* 57, 194–204. doi:10.1016/j.culher.2022.08.013

Albéric, M., Gourrier, A., Wagermaier, W., Fratzl, P., and Reiche, I. (2018). The three-dimensional arrangement of the mineralized collagen fibers in elephant ivory and its relation to mechanical and optical properties. *Acta Biomater.* 72, 342–351. doi:10.1016/j.actbio.2018.02.016

Anczkiewicz, R., Nava, A., Bondioli, L., Müller, W., Spötl, C., Koziarska, M., et al. (2023). High spatial resolution Sr isotope and trace element record of dental enamel mineralization in a woolly mammoth tooth: implications for paleoecological reconstructions. *Quat. Sci. Rev.* 313, 108191. doi:10.1016/j.quascirev.2023.108191

Bandara, T., Xu, J., Potter, I. D., Franks, A., Chathurika, J. B. a.J., and Tang, C. (2020). Mechanisms for the removal of Cd (II) and Cu (II) from aqueous solution and mine water by biochars derived from agricultural wastes. *Chemosphere* 254, 126745. doi:10.1016/j.chemosphere.2020.126745

Beasley, M. M., Bartelink, E. J., Taylor, L., and Miller, R. M. (2014). Comparison of transmission FTIR, ATR, and DRIFT spectra: implications for assessment of bone bioapatite diagenesis. *J. Archaeol. Sci.* 46, 16–22. doi:10.1016/j.jas.2014.03.008

Brody, R. H., Edwards, H. G., and Pollard, A. M. (2001). Chemometric methods applied to the differentiation of Fourier-transform Raman spectra of ivories. *Anal. Chim. Acta* 427 (2), 223–232. doi:10.1016/s0003-2670(00)01206-x

Bronk Ramsey, C. (2016). Bayesian analysis of radiocarbon dates. *Radiocarbon* 51 (1), 337–360. doi:10.1017/s0033822200033865

Chi, X. (2013). An explication of the emperor scepter symbol of ancient babylon and ancient China with oraclebone and bronze inscriptions and relics in Sanxingdui ruins. *Chin. Semiot. Stud.* 9 (1), 126–142. doi:10.1515/css-2013-0110

De Flamingh, A., Coutu, A., Sealy, J., Chirikure, S., Bastos, A. D. S., Libanda-Mubusisi, N. M., et al. (2020). Sourcing elephant ivory from a Sixteenth-Century Portuguese shipwreck. *Curr. Biol.* 31 (3), 621–628.e4. doi:10.1016/j.cub.2020.10.086

Doménech-Carbó, M. T., Buendía-Ortuño, M., Pasies-Oviedo, T., and Osete-Cortina, L. (2016). Analytical study of waterlogged ivory from the Bajo de la campana site (Murcia, Spain). *Microchem. J.* 126, 381–405. doi:10.1016/j.microc.2015.12.022

Durga, R., Jimenez, N., Ramanathan, S., Suraneni, P., and Pestle, W. J. (2022). Use of thermogravimetric analysis to estimate collagen and hydroxyapatite contents in archaeological bone. *J. Archaeol. Sci.* 145, 105644. doi:10.1016/j.jas.2022.105644

Elliott, J. C. (1969). Recent progress in the chemistry, crystal chemistry and structure of the apatites. *Calcif. Tissue Res.* 3, 293–307. doi:10.1007/bf02058672

Figueiredo, M., Fernando, A., Martins, G., Freitas, J., Judas, F., and Figueiredo, H. (2010). Effect of the calcination temperature on the composition and microstructure of hydroxyapatite derived from human and animal bone. *Ceram. Int.* 36, 2383–2393. doi:10.1016/j.ceramint.2010.07.016

Godfrey, I. M., Ghisalberti, E. L., Beng, E. W., Byrne, L. T., and Richardson, G. W. (2002). The analysis of ivory from a Marine environment. *Stud. Conserv.* 47 (1), 29–45. doi:10.1179/sic.2002.47.1.29

Guan, Y., Hua, Z., Cheng, Y., He, J., Zhang, Y., and Guan, J. (2023). Monitoring of water content of apple slices using low-field nuclear magnetic resonance during drying process. *J. Food Process Eng.* 46 (12), e14445. doi:10.1111/jfpe.14445

Guo, J., Chen, J., Li, R., Liu, J. A., Luo, R., Jiao, L., et al. (2022). Thermoporometry of waterlogged archaeological wood: insights into the change of pore traits after the water-removal by supercritical drying. *Thermochim. Acta* 715, 179297. doi:10.1016/j.tca.2022.179297

Guo, Y., Xiang, F., Ran, H., Xie, Z., Yang, Q., Huang, H., et al. (2023). The sacrificial record in burial pits of the late Shang Dynasty: evidences from the chroma and magnetic properties of the Sanxingdui site, Sichuan, China. *Herit. Sci.* 11 (1), 258. doi:10.1186/s40494-023-01105-0

Hinshaw, S., and Wohl, E. (2021). Quantitatively estimating carbon sequestration potential in soil and large wood in the context of river restoration. *Front. Earth Sci.* 9, 708895. doi:10.3389/feart.2021.708895

Islam, M., Mishra, P. C., and Patel, R. (2011). Arsenate removal from aqueous solution by cellulose-carbonated hydroxyapatite nanocomposites. *J. Hazard. Mater.* 189 (3), 755–763. doi:10.1016/j.jhazmat.2011.03.051

Jackes, M., Sherburne, R., Lubell, D., Barker, C., and Wayman, M. (2001). Destruction of microstructure in archaeological bone: a case study from Portugal. *Int. J. Osteoarchaeol.* 11 (6), 415–432. doi:10.1002/oa.583

Jantou-Morris, V., Horton, M. A., and Mccomb, D. W. (2010). The nano-morphological relationships between apatite crystals and collagen fibrils in ivory dentine. *Biomaterials* 31, 5275–5286. doi:10.1016/j.biomaterials.2010.03.025

Jaswal, A., Samir, S., and Manna, A. (2023). Synthesis of nanocrystalline hydroxyapatite biomaterial from waste eggshells by precipitation method. *T. Indian i. Met.* 76, 2221–2230. doi:10.1007/s12666-023-02937-x

Jingsong, S. (2005). Re-examination of the artifact pits of Sanxingdui. *Chin. Archaeol.* 5 (1), 200–208. doi:10.1515/CHAR.2005.5.1.200

Kostov-Kytin, V. V., Dyulgerova, E., Ilieva, R., and Petkova, V. (2018). Powder X-ray diffraction studies of hydroxyapatite and β-TCP mixtures processed by high energy dry milling. *Ceram. Int.* 44, 8664–8671. doi:10.1016/j.ceramint.2018.02.094

Kuila, U., and Prasad, M. (2013). Specific surface area and pore size distribution in clays and shales. *Geophys. Prospect.* 61, 341–362. doi:10.1111/1365-2478.12028

Lai, C. (2015). Archaeological museums and tourism in China: a case study of the Sanxingdui museum. *Mus. Manage. Curator.* 30, 75–93. doi:10.1080/09647775.2015.1008391

Lao, G., Zhou, Z., Wu, R., Wang, C., Wu, W., Lv, S., et al. (2024). Exploring the key deteriorative microorganisms on ancient ivories unearthed from the Sanxingdui Ruins site during temporary cold storage. *Front. Microbiol.* 15, 1400157. doi:10.3389/fmicb.2024.1400157

Lebon, M., Reiche, I., Fröhlich, F., Bahain, J. J., and Falguères, C. (2008). Characterization of archaeological burnt bones: contribution of a new analytical protocol based on derivative FTIR spectroscopy and curve fitting of the v_1 v_3 PO_4 domain. *Anal. Bioanal. Chem.* 392, 1479–1488. doi:10.1007/s00216-008-2469-y

Li, R., Guo, J., Macchioni, N., Pizzo, B., Xi, G., Tian, X., et al. (2022). Characterisation of waterlogged archaeological wood from Nanhai No. 1 shipwreck by multidisciplinary diagnostic methods. *J. Cult. Herit.* 56, 25–35. doi:10.1016/j.culher.2022.05.004

Li, X., Wang, C., Zhang, Y., Zhang, R., Li, S., Xiao, Q., et al. (2023). Fourier-transformed infrared spectroscopy study of the ancient ivory tusks from the Sanxingdui site. *Front. Earth Sci.* 10, 1008139. doi:10.3389/feart.2022.1008139

Liu, S., Li, Y., Sun, H., Zhang, S., Zeng, X., Zong, P., et al. (2018). Preparation and characterisation of a lamellar hydroxyapatite/polylactic acid composite. *Plast. Rubber Compos.* 48, 66–73. doi:10.1080/14658011.2018.1548191

Locke, M. (2008). Structure of ivory. *J. Morphol.* 269, 423–450. doi:10.1002/jmor.10585

López-Costas, O., Lantes-Suárez, Ó., and Martínez Cortizas, A. (2016). Chemical compositional changes in archaeological human bones due to diagenesis: type of bone vs soil environment. *J. Archaeol. Sci.* 67, 43–51. doi:10.1016/j.jas.2016.02.001

Lu, Y., Jiao, L., Sun, G., Wang, J., Liu, S., Li, R., et al. (2023). Preservation status and microbial community of waterlogged archaeological woods over 7,800 years old at the Jingtoushan Site, China. *Wood Sci. Technol.* 57, 537–556. doi:10.1007/s00226-023-01463-9

Lv, C., Tian, H., Zhang, X., and Xiang, A. (2018). LF-NMR analysis of the water mobility, state and distribution in sorbitol plasticized polyvinyl alcohol films. *Polym. Test.* 70, 67–72. doi:10.1016/j.polymertesting.2018.06.024

Marcomini, A. L., Rego, B. T., and Suman Bretas, R. E. (2016). Improvement of the short- and long-term mechanical properties of injection-molded poly(etheretherketone) and hydroxyapatite nanocomposites. *J. Appl. Polym. Sci.* 134 (7). doi:10.1002/app.44476

Montoya-Escobar, N., Ospina-Acero, D., Velásquez-Cock, J. A., Gómez-Hoyos, C., Serpa Guerra, A., Gañan Rojo, P. F., et al. (2022). Use of fourier series in X-ray Diffraction (XRD) analysis and Fourier-Transform Infrared Spectroscopy (FTIR) for estimation of crystallinity in cellulose from different sources. *Polymers* 14 (23), 5199. doi:10.3390/polym14235199

Papynov, E. K., Portnyagin, A. S., Modin, E. B., Mayorov, V. Y., Shichalin, O. O., Golikov, A. P., et al. (2018). A complex approach to assessing porous structure of structured ceramics obtained by SPS technique. *Mater. Charact.* 145, 294–302. doi:10.1016/j.matchar.2018.08.044

Pebriani, C. P., Nurlely, and Sari, Y. W. (2019). Microwave–assisted precipitation of carbonated hydroxyapatite. *J. Phys. Conf. Ser.* 1248 (1), 012078. doi:10.1088/1742-6596/1248/1/012078

Penvern, H., Zhou, M., Maillet, B., Courtier-Murias, D., Scheel, M., Perrin, J., et al. (2020). How bound water regulates wood drying. *Phys. Rev. Appl.* 14 (5), 054051. doi:10.1103/PhysRevApplied.14.054051

Piccini, L., Nannoni, A., Costagliola, P., Paolieri, M., and Vigiani, C. (2021). Composition and structure of phosphate-rich parietal crusts and nodules in monte corchia cave, alpi apuane (Central Italy). *Front. Earth Sci.* 9, 673109. doi:10.3389/feart.2021.673109

Rabiei, M., Palevicius, A., Monshi, A., Nasiri, S., Vilkauskas, A., and Janusas, G. (2020). Comparing methods for calculating nano crystal size of natural hydroxyapatite using X-ray diffraction. *Nanomaterials* 10 (9), 1627. doi:10.3390/nano10091627

Reimer, P. J., Austin, W. E. N., Bard, E., Bayliss, A., Blackwell, P. G., Bronk Ramsey, C., et al. (2020). The IntCal20 Northern Hemisphere radiocarbon age calibration curve (0–55 cal kBP). *Radiocarbon* 62 (4), 725–757. doi:10.1017/rdc.2020.41

Scaggion, C., Dal Sasso, G., Nodari, L., Pagani, L., Carrara, N., Zotti, A., et al. (2024). An FTIR-based model for the diagenetic alteration of archaeological bones. *J. Archaeol. Sci.* 161, 105900. doi:10.1016/j.jas.2023.105900

Shen, M., Lu, Z., Xu, Y., and He, X. (2021). Vivianite and its oxidation products in mammoth ivory and their implications to the burial process. *ACS Omega* 6, 22284–22291. doi:10.1021/acsomega.1c02964

Sun, J., Zhou, L., Han, P., and Qiao, G. (2023). UV-Initiated frontal polymerization for the fast synthesis of bubble-free, self-propagating hydrogel anticorrosive coatings. *ACS Appl. Mater. Interfaces* 15, 28618–28625. doi:10.1021/acsami.3c04870

Sun, X., He, M., and Wu, J. (2022). Crystallographic characteristics of inorganic mineral in mammoth ivory and ivory. *Minerals* 12 (2), 117. doi:10.3390/min12020117

Tranchant, L., Müller, K., Lemasson, Q., Pichon, L., Schöder, S., Conard, N. J., et al. (2023). Improved discrimination of biogenic and diagenetic elements in palaeolithic mammoth ivory and bone from hohle fels cave in the swabian jura of southwestern Germany. *Quatern. Int.* 660, 4–12. doi:10.1016/j.quaint.2023.02.006

Valášek, V., Pachnerová Brabcová, K., Kufnerová, J., Molnár, M., and Světlík, I. (2022). Refining radiocarbon dating of ivory. *Radiat. Prot. Dosim.* 198, 675–680. doi:10.1093/rpd/ncac118

Van Rijt, M. M. J., Nooteboom, S. W., Van Der Weijden, A., Noorduin, W. L., and De With, G. (2021). Stability-limited ion-exchange of calcium with zinc in biomimetic hydroxyapatite. *Mater. Des.* 207, 109846. doi:10.1016/j.matdes.2021.109846

Vargas-Becerril, N., García-García, R., and Reyes-Gasga, J. (2018). Structural changes in human teeth after heating up to 1200 °C in argon atmosphere. *Mat. Sci. Appl.* 9 (7), 637–656. doi:10.4236/msa.2018.97046

Virág, A. (2012). Histogenesis of the unique morphology of proboscidean ivory. *J. Morphol.* 273, 1406–1423. doi:10.1002/jmor.20069

Volkov, M., Turanova, O., and Turanov, A. (2018). Determination of moisture content of insulating oil by NMR method with selective pulses. *IEEE T. Dielect. El.* 25, 1989–1991. doi:10.1109/tdei.2018.007342

Xia, X., Shen, J., Cao, F., Wang, C., Tang, M., Zhang, Q., et al. (2019). A facile synthesis of hydroxyapatite for effective removal strontium ion. *J. Hazard. Mater.* 368, 326–335. doi:10.1016/j.jhazmat.2019.01.040

Xu, J.-W., Li, C.-C., Hung, K.-C., Chang, W.-S., and Wu, J.-H. (2022). Physicomechanical properties of hydrothermally treated Japanese cedar timber and their relationships with chemical compositions. *J. Mater. Res. Technol.* 21, 4982–4993. doi:10.1016/j.jmrt.2022.11.092

Xu, X., Wang, K., Tan, X., Zhang, L., and Liu, L. (2024). Osteo-angiogenic activity of a micro/nano hierarchical SrSi-codoped hydroxyapatite coating on zirconium alloy. *J. Mater. Res. Technol.* 30, 6924–6940. doi:10.1016/j.jmrt.2024.05.067

Yan, L., Qian, C., Xin, Y., and Li, D. (2022). Adsorption characteristics and pore structure of organic-rich shale with different moisture contents. *Front. Earth Sci.* 10, 863691. doi:10.3389/feart.2022.863691

Yan, W., Sun, J., Sun, Y., and Golsanami, N. (2018). A robust NMR method to measure porosity of low porosity rocks. *Micropor. Mesopor. Mat.* 269, 113–117. doi:10.1016/j.micromeso.2018.02.022

Yang, S., and Xu, X. (2022). Bronze masks of mysterious Sanxingdui: oldest record of Graves' disease? *J. Endocrinol. Invest.* 45, 1115–1116. doi:10.1007/s40618-021-01643-z

Yu, Q., Liu, H., Lv, G., Liu, X., Wang, L., and Liao, L. (2023). Mechanistic insight into lead immobilization on bone-derived carbon/hydroxyapatite composite at low and high initial lead concentration. *Sci. Total Environ.* 900, 165910. doi:10.1016/j.scitotenv.2023.165910

Zhang, Y., Li, Q., Hu, Q., Zhai, C., Song, M., Xu, J., et al. (2022). Pore wetting process characterization of equal-sized granular coals by using LF-NMR technology. *Fuel* 313, 122670. doi:10.1016/j.fuel.2021.122670

Zheng, B., Luo, Y., Liao, H., and Zhang, C. (2017). Investigation of the crystallinity of suspension plasma sprayed hydroxyapatite coatings. *J. Eur. Ceram. Soc.* 37, 5017–5021. doi:10.1016/j.jeurceramsoc.2017.07.007

Zheng, W., Li, X., Lam, N., Wang, X., Sun, Z., Liu, S., et al. (2013). Application of multi-frequency electromagnetic profiling in studying the distribution of bronze in Jinsha ruin worship. *Int. J. Smart Sens. Int.* 6, 733–751. doi:10.21307/ijssis-2017-563

Zhu, J., Li, S., Yang, L., Zhao, Z., Xia, J., Zhu, Y., et al. (2023). Effect of multiple freeze–thaw cycles on water migration, protein conformation and quality attributes of beef longissimus dorsi muscle by real-time low field nuclear magnetic resonance and Raman spectroscopy. *Food Res. Int.* 166, 112644. doi:10.1016/j.foodres.2023.112644

Zhu, Y., Ju, R., Ma, F., Qian, J., Yan, J., Li, S., et al. (2021). Moisture variation analysis of the green plum during the drying process based on low-field nuclear magnetic resonance. *J. Food Sci.* 86, 5137–5147. doi:10.1111/1750-3841.15955